Geochimica et Cosmochimica Acta, Vol. 69, No. 17, pp. 4349–4360, 2005

0016-7037/05 $30.00 + .00

doi:10.1016/j.gca.2004.11.025

Partitioning of Cu, Ni, Au, and platinum-group elements between monosulfide solid solution and sulfide melt under controlled oxygen and sulfur fugacities

James E. Mungall,[1,*] David R. A. Andrews,[1] Louis J. Cabri,[2,3] Paul J. Sylvester,[4] and Michael Tubrett[4]

[1]Department of Geology, University of Toronto, 22 Russell St., Toronto, ON M5S 3B1, Canada
[2]Canada Centre for Mineral and Energy Technology, 555 Booth Street, Ottawa, ON K1A 0G1, Canada
[3]Department of Earth Sciences, Memorial University of Newfoundland, St. John's, NF A1B 3X5, Canada
[4]Department of Earth Sciences, Memorial University of Newfoundland, St. John's, NF A1B 3X5, Canada

(*Received February* 10, 2004; *accepted in revised form November* 2, 2004)

Abstract—We have performed six experiments in which we equilibrated monosulfide solid solution (mss) with sulfide melt in evacuated silica capsules containing solid buffers to fix oxygen and sulfur fugacity, at temperatures of 950°C, 1000°C and 1050°C at bulk concentrations of ~50 ppm for each of the PGE and Au, 5% Ni, and 7% Cu. Concentrations of O, S, Fe, Ni and Cu were determined by electron microprobe, whereas precious metal concentrations were determined by laser-ablation inductively-coupled mass spectrometry. Partition coefficients of all elements studied show minimal dependences on oxygen fugacity from the IW to the QFM buffers when sulfur fugacity is fixed at the Pt-PtS buffer. Cu, Pt, Pd and Au are strongly incompatible and Ru remains moderately to strongly compatible under all conditions studied. At all oxygen fugacities, at the Pt-PtS sulfur buffer, Ir and Rh remain highly compatible in mss. In the single run at both low oxygen and low sulfur fugacity Ir and Rh were found to be strongly incompatible in mss. At QFM and Pt-PtS the partition coefficient for Ni shows weak temperature dependence, ranging from 0.66 at 1050°C to 0.94 at 950°C. At lower oxygen and sulfur fugacity Ni showed much more incompatible behavior. Comparison with the compositions of sulfide ores from the Lindsley deposit of Sudbury suggests that the sulfide magma evolved under conditions close to the QFM and Pt-PtS buffers. The compatible behavior observed for Ni, Ir and Rh at Lindsley and most other magmatic sulfide deposits hosted by mafic rocks requires equilibration of mss and sulfide liquid at moderately high sulfur fugacity and low temperatures near to the solidus of the sulfide magma. We argue that this constraint requires that the sulfide magma must have evolved by equilibrium crystallization, rather than fractional segregation of mss as is commonly supposed.

1. INTRODUCTION

One of the main controls on the diversity of compositions and mineralogy of magmatic sulfide deposits involves crystallization of monosulfide solid solution (mss) from a sulfide liquid (e.g., Hawley, 1965; Naldrett and Kullerud, 1967; Craig and Kullerud, 1969; Naldrett, 1969; Li et al., 1992; Naldrett et al., 1994, 1999; Zientek et al., 1994). Here we present new experimental constraints on the partitioning of base metals Ni and Cu and precious metals Ir, Ru, Rh, Pt, Pd, (platinum-group elements; PGE) and Au between mss and sulfide liquid in the system Fe-Ni-Cu-PGE-Au-S-O. The key difference between this study and several other recent ones is that we have equilibrated oxygen-bearing sulfide liquid with mss at known fO_2 and fS_2 whereas previous investigators have worked in oxygen-free systems without explicit control of fS_2. The experiments conducted in this study serve to link the previously known compositional and temperature dependences of partition coefficients to the intensive parameters of the system, allowing broader application of the entire database.

2. PREVIOUS WORK

In several studies, investigators have equilibrated mss and sulfide melt in the systems Fe-Ni-S (Distler et al., 1977; Fleet and Stone, 1991; Fleet et al., 1999b), Fe-Ni-Cu-S (Fleet et al., 1993, 1999a; Fleet and Pan, 1994; Ebel and Naldrett, 1996; Li et al., 1996; Ballhaus et al., 2001; Barnes et al., 2001; Makovicky, 2002). In each case, results can be used to establish a partitioning coefficient D_i for each element, defined as the concentration of the element in mss divided by its concentration in coexisting sulfide liquid (Fleet et al., 1999b). The most significant results of these studies are as follows. In all systems studied, D_{Cu} is between 0.2 and 0.3 under most conditions. D_{Pt}, D_{Pd}, and D_{Au} are all much <1, leading to their concentration in the liquid during mss crystallization. In S-rich systems Ir, Os, Ru and Rh are highly compatible with mss, whereas with decreasing S-content in the liquid, the partition coefficients decrease until, in alloy-saturated systems, only Ru remains compatible in mss. Ni behaves in a manner similar to Ir, Os, Ru and Rh, with D_{Ni} being a strong positive function of sulfur content of the liquid, but D_{Ni} also shows significant temperature dependence unlike the other elements. Ni shows compatible behavior only under the most S-rich conditions at very low temperatures close to the solidus temperature of natural sulfide magmas. In general, the logarithms of partition coefficients appear to follow linear dependences on the sulfur content of the liquid (e.g., Barnes et al., 1997).

The results summarized above can be used to predict qualitatively the behavior of most base and precious metals in natural sulfide deposits, and models of fractional crystallization of mss are popular (e.g., Hawley, 1965; Naldrett and Kullerud, 1967; MacLean, 1969; Craig and Kullerud, 1969; Naldrett,

* Author to whom correspondence should be addressed (mungall@geology.utoronto.ca).
† *Present address:* Inco Technical Services, Hwy. 17 W, Coppercliff, ON P0M 1NO, Canada.

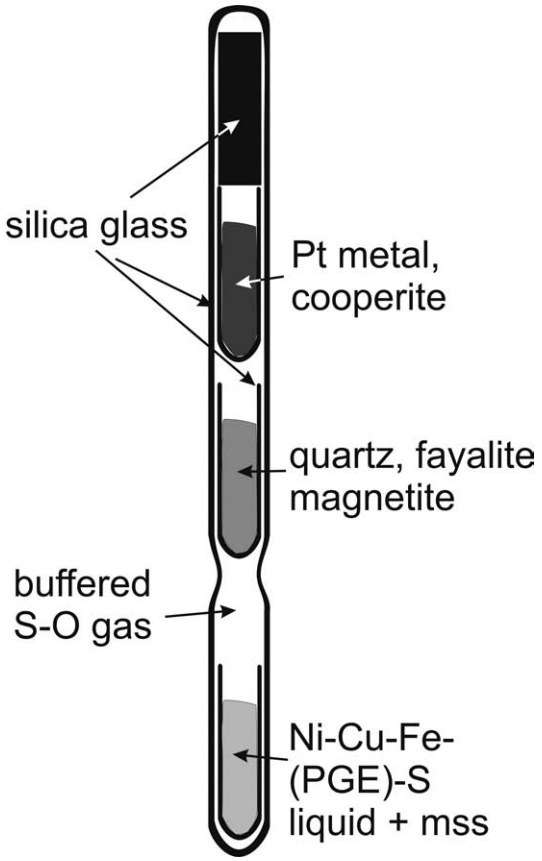

Fig. 1. Experimental configuration.

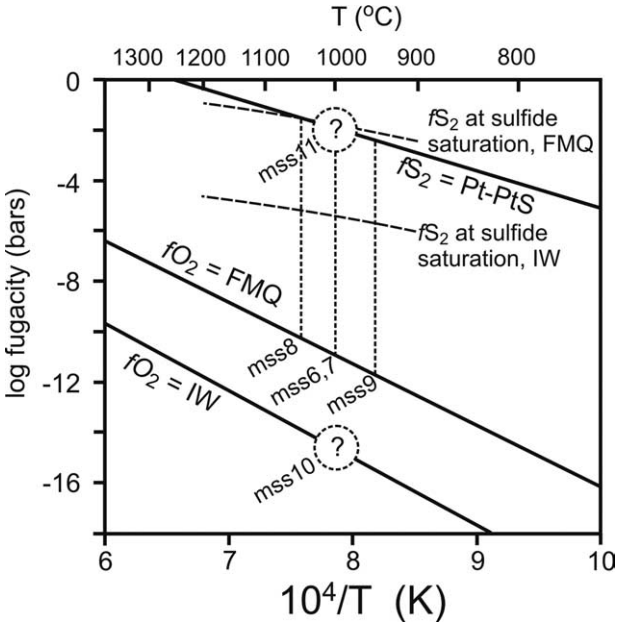

Fig. 2. Summary of experimental conditions. Dashed vertical lines join conditions of sulfur and oxygen fugacities of individual runs where both parameters were buffered. Runs for which only one parameter was buffered are shown as dashed circles. The nearly horizontal dashed curves indicate the sulfur fugacity at which a basaltic liquid containing ~10 mol.% FeO will be saturated with sulfide according to Wallace and Carmichael (1992), for a given oxygen fugacity. The conditions of mss6, 7, 8 and 9 are close to those expected for sulfide equilibrated with a natural basaltic magma with normal oxygen fugacity.

1969; Li et al., 1992; Naldrett et al., 1994, 1999; Zientek et al., 1994). There two serious shortcomings of the existing database that hinder its application to natural systems. First, apart from the early work of MacLean (1969), Naldrett (1969), Doyle and Naldrett (1987) and more recent studies by Kress (1997), none of the experiments were conducted in the presence of oxygen despite the fact that oxygen is a major element in natural sulfides, some of which contain several wt.% O and most of which crystallize magnetite as a liquidus phase. In those studies that were conducted with oxygen present, the metals Ni, Cu, Au, and PGE were not present, precluding any direct assessment of the controls exerted on partitioning by oxygen content of the liquid. None of the experiments directed at measurement of partition coefficients were conducted under conditions of known oxygen or sulfur fugacity. It has hitherto therefore been impossible to apply known dependences of partition coefficients upon S content of the melt to quantitative models of sulfide magma evolution constrained by externally imposed intensive parameters.

3. EXPERIMENTAL METHODS

3.1. Experimental Setup

The experimental design is illustrated in Figure 1. Starting materials were placed in the bases of the silica tubes, which had previously been closed at one end and crimped partly shut 5 to 8 mm above their bases. Above the starting materials, two smaller silica cups were placed, one holding a solid assemblage chosen to buffer oxygen fugacity, the other a solid sulfur fugacity buffer. A silica spacer rod sat atop the upper buffer cup, to separate it from the heat applied during evacuation and fusion of the upper seal on the outer capsule. Experiments were conducted by suspending the sealed silica tubes in a vertical tube furnace or by placing them inside a large alumina crucible in a top-loading pot furnace. The temperature gradient across the 4 to 5 cm length of the capsules was <5°C, as measured by passing a Pt-$Pt_{90}Rh_{10}$ thermocouple through the hot zone of the furnace. After completion of each run the charge was removed from the furnace and quenched into a container of cold water.

Oxygen and sulfur fugacities were controlled with solid assemblages of quartz+fayalite+magnetite (the QFM fO_2 buffer) and Pt-PtS (the PtS fS_2 buffer). We assume that the vapor phase filling the space between the main capsule and the two buffer capsules remained simultaneously in equilibrium with the contents of all three capsules. In this way the fO_2 and fS_2 of the sulfide assemblage was held at fixed and calculable levels throughout the experiments. This approach required some initial adjustments, to ensure that the initial sulfide composition was sufficiently close to its desired composition that it did not consume one or both buffers. In Figure 2 we illustrate the oxygen and sulfur fugacities of the QFM, IW (Fe-FeO) and PtS buffers over the temperature range of our experiments, calculated using thermochemical data from Barin (1995).

3.2. Synthesis of Starting Materials

The starting materials for our experiments were synthesized by mixing powdered high-purity metals and sulfur (Alfa Aesar 99.9% Cu, 99.997% Fe_3O_4, 99.999% Pt, 99.95% Rh, 99.95% Ru, 99.995% Ir, 99.95% Os; Aldrich 99.999% N, 99.999% Pd, 99.999% S). An initial mixture of $Fe_{49}S_{35}Ni_{5.3}Cu_{7.6}$ and ~0.5% each of Pt, Pd, Rh, Ru, Os, Ir and Au was ground in an agate mortar and pestle under ethanol and dried. The powder was added to a silica tube with a silica rod spacer on the top, and the tube was sealed under vacuum. The silica capsule was placed in the hot zone of a vertical tube furnace at 900°C and ramped

Table 1. Nominal and measured concentrations of base and precious metals in experimental starting materials. Methods are described in the text.

Element	Nominal concentration	DA121702A	DA121702B	DA121702D	Blank
Fe (wt.%)	51.06				
S (wt.%)	36.61				
Ni (wt.%)	5.41				
Cu (wt.%)	6.89				
Pt (ppm)	43.4	41	44.4	45.7	0
Pd (ppm)	41.2	34.5	33.6	33.7	0.1
Rh (ppm)	34.7	22.9	22.7	22.5	0
Ru (ppm)	23.9	32.5	32.2	31.8	0
Os (ppm)	47.8				
Ir (ppm)	30.4	24.9	26.7	26.7	0
Au (ppm)	49.9	79.5	86.7	89	37.1
Au-blank	n.a.		42.4	49.6	51.9
Total	99.97				

to 1000°C over 1 h, then left for 17 h before being dropped into cold water. The quenched sulfide was recovered and reground under ethanol, whereupon 5.4 g of this material was added to 498 g of a mixture of elemental weight composition $Fe_{51}S_{37}Ni_5Cu_7$. The resulting mixture was again sealed under vacuum, and held in a bottom-loading furnace at 1175°C for 20 min. Quenched sulfide recovered from this second fusion was ground and used as the starting material for all of the experiments reported in this study.

Three ~10-mg aliquots of the starting mixture and one blank were placed separately in Teflon beakers and digested in 62 mL each of hot 9.2% aqua regia (6 mL HCl, 2 mL HNO_3, 54 mL deionized water). The resulting solutions were analyzed by ICPMS at Activation Laboratories Ltd, Ancaster ON. In Table 1, we present the nominal composition of the sulfide starting mixture (as weighed in), and the concentrations of Ru, Rh, Pd, Ir and Pt as measured in the three digested samples. The discrepancies between nominal and measured compositions result from the fact that measured weights of the precious metals in the original mixture were only approximative, our intention being to measure them accurately after synthesis was complete. The measured concentration of Au in the digested starting materials and the blank is very high, but if the blank is subtracted from the measured values the result is close to the nominal composition. S and O contents of the experimental charges varied through reaction with the buffer assemblages, but the metal ratios in the bulk experimental charges are assumed to have remained constant. In any case, we are interested in precise determination of partitioning at trace abundances rather than knowing the precise concentrations in the bulk experimental charges.

3.3. Analytical Methods

Run products were mounted in epoxy, sectioned, and polished for microscopic examination and microanalysis of quenched phases. Fe, Ni, Cu, S, and O concentrations were determined at the University of Toronto using a Cameca SX50 electron microprobe (EMP) with three wavelength-dispersive spectrometers. The instrument was operated with a 20-kV accelerating voltage, 60-nA beam current, and with the beam defocused to a 30-μm diameter. O was determined using a synthetic ODPB pseudocrystal in the wavelength-dispersive spectrometer. Measurement of O is difficult by EMP due to the extreme attenuation of the low-energy O Kα X-rays by the matrix and even by the carbon coating used to conduct charge away from the analysis spot. To overcome these difficulties we repolished the hematite O standard between uses, and carbon-coated the standard and unknowns together immediately before each analytical session. The steeply sloping background in the vicinity of the O Kα peak was approximated with a parabolic fitting function. Although most quenched sulfide liquids consisted of intergrowths of mss and another, more Cu-rich phase, we have found that averaging of several spot analyses gives highly reproducible results, as is shown in the following section.

Concentrations of the precious metals Ir, Ru, Rh, Pt, Pd, and Au were determined at Memorial University of Newfoundland (MUN) using laser-ablation inductively-coupled plasma mass spectrometry (LA-ICPMS). Os could not be analysed using the equipment available. The system is a Fisons VG PlasmaQuad 2S+ ICP-MS instrument coupled to an in-house built 266 nm NdYAG laser. Ablations were performed in helium carrier gas, which was combined with argon just before the feed to the torch. Nebulizer flow rates were 0.91 L/min He and 0.79 L/min Ar. The laser beam was focused 100 μm above the sample with an energy of 0.4 mJ/pulse (measured just before the beam enters the objective of the microscope), and a laser repetition rate of 10 Hz, producing an ~50-μm diameter spot on the sample. Time resolved intensity data were acquired by peak-jumping in pulse-counting mode with one point measured per peak for masses 7 (Li: fly back peak, used to increase the quadrupole settling time after the jump from high to low mass in each sweep), 33 and 34 (S), 55 (Mn), 57 (Fe), 59 (Co), 61 (Ni), 65 (Cu), 66 and 68 (Zn), 87 (Sr), 90 (Zr), 95 (Mo), 99, 101 and 102 (Ru), 103 (Rh), 105, 106 and 108 (Pd), 111 (Cd), 178 (Hf), 181 (Ta), 191 and 193 (Ir), 194 and 195 (Pt) and 197 (Au). The internal standard element was S (using mass 34), whose concentration was determined from EMPA. Masses representing Mn, Fe, Co, Ni, Cu, Zn, Sr, Zr, Mo, Cd, Hf and Ta were monitored for possible spectral interferences on the masses of the precious metals (see below). Quadrupole settling time was 1 ms and the dwell time was 8.3 ms on each mass. Approximately 60 s of gas background data (with the laser beam blocked) were collected before each 60-s ablation of standards and unknowns.

Two fused, synthetic sulfide materials, Po-30 and Po-689, with a pyrrhotite matrix, were used for concentration calibrations. Both standards were synthesized by fusion in evacuated double silica glass tubes following the methods described by Cabri et al. (2003). The Po-30 standard contains ~4 to 11 ppm of each of Ru, Rh, Pd, Ir and Pt, as calibrated against the sintered, synthetic sulfide standards of Ballhaus and Sylvester (2000) and the Po-689 standard contains ~10 ppm Au, as calibrated against standard MASS-1 (Wilson et al., 2002). Data were reduced using MUN's in-house CONVERT and LAMTRACE spreadsheet programs, which employ procedures described by Longerich et al. (1996). The error for the method is estimated to be better than 10% relative based on the reproducibility of results for various reference materials measured from day to day over several months in our laboratory. Limits of detection were typically <0.1 ppm for the light PGE and <0.01 ppm for the heavy PGE.

Corrections for isobaric overlaps of ^{102}Pd on ^{102}Ru, ^{106}Cd on ^{106}Pd, ^{108}Cd on ^{108}Pd, ^{63}Cu^{40}Ar on ^{103}Rh, and ^{65}Cu^{40}Ar on ^{105}Pd were made using the algorithms described by Sylvester (2001). These amounted to 0 to 1.5%, 0 to 5.5%, 0 to 2.9%, 2 to 14%, 25 to 88%, respectively, for mss crystals, and 6 to 78%, <0.1%, <0.1%, 21 to 87%, 20 to 40%, respectively, for quenched melts. In the case of the melt for mss8, the estimated signal for ^{63}Cu^{40}Ar was comparable to that measured at mass 103 and so the Rh concentration could not be estimated accurately in analyses of this material. Count rates for Ni were significant (3–20 $\times$ 10^4 for mass 61) in all samples so it is likely that there was some contribution of ^{61}Ni^{40}Ar to ^{101}Ru or ^{62}Ni^{40}Ar to ^{102}Ru in the analyses. However, we were not able to monitor the nickel argide production rate

accurately during this study so corrections could not be made to the ^{101}Ru or ^{102}Ru data. The interferences are probably minor because data for the ^{101}Ru or ^{102}Ru isotopes yield concentrations similar to that derived from the ^{99}Ru isotope. The latter isotope was not affected by interference of ^{59}Co^{40}Ar in this study because measured count rates for cobalt were negligible in all samples.

3.4. Experimental Conditions

After a number of reconnaissance runs, six successful experiments were conducted under the conditions listed in Table 2. The temperature range from 1050 to 950°C was chosen to cover most of the crystallization interval of natural sulfide magmas. Runs mss6, mss7, mss8, and mss9 were conducted at the QFM oxygen buffer and the Pt-PtS sulfur buffer, whereas mss10 and mss11 were attempts to work at the iron-wüstite (IW) oxygen fugacity buffer and Pt-PtS sulfur buffer. We were only partly successful in the latter attempt; in experiment mss10 the PtS was all consumed by transfer of S to the sulfide melt through the vapor phase, so that the run was conducted at an unbuffered fS_2 below Pt-PtS and at oxygen fugacity fixed at the IW buffer. In run mss11 the alloy in the starting oxygen buffer was entirely oxidized to wüstite, leaving the oxygen fugacity of the system unbuffered between the IW and wüstite-magnetite buffers and sulfur fugacity fixed at the Pt-PtS buffer.

Experiments mss6 and mss7 were done at the same conditions (1000°C, Pt-PtS, QFM) for 2 and 13 d, respectively, in an attempt to demonstrate that equilibrium had been attained. Although there are small differences between the compositions of the two runs, presumably due to inhomogeneity of the powdered sulfide starting material, the partition coefficients calculated for both experiments are very similar, as described in the following section. We take this observation to mean that the compositions of coexisting phases did not change after the first 2 d, and that equilibrium had probably been attained in all runs of >2 d in duration. All subsequent runs lasted for at least 3.5 d.

4. RESULTS

The product of a typical run is illustrated in Figure 3. Crystallization of the amorphous silica capsule wall formed a crust of quartz crystals along the interior, but most of the capsule remained in the glassy state. Ovoid crystals of mss are surrounded by quenched sulfide liquid, which crystallized to a fine trellis-textured intergrowth of mss and Cu-rich phases during quench. Bubbles of a vapor, presumably in the S-O system, formed during the quench in some charges, forming rounded cavities between the mss crystals and expelling the remaining melt outward. Although some of the vapor bubbles are impressively large, the vapor phase has such low density compared with that of the condensed phases that these voids actually represent very small amounts of lost material. Microprobe traverses of mss crystals and quenched liquid away from the vapor bubbles suggested that minor amounts of degassing of S from mss crystals occurred during cooling. We therefore avoided analyzing the margins of mss crystals.

The solid buffer assemblages were checked after each experiment by visual inspection and X-ray diffraction to verify that the desired phases were still present. In experiments mss10 and mss11, the solid oxygen buffer reacted with the vapor in the capsule to produce a mixture of wüstite, quartz, and Fe-S-O melt. Alloy also was present in the oxygen buffer in experiment mss10, but not in mss11.

The results of the six successful experiments are summarized in Table 2 as the averages of at least 8 and usually ~25 individual microprobe spots (major elements) and three to four individual LA-ICPMS analyses along with detection limits, standard deviations, and calculated values of D for each element analyzed.

5. DISCUSSION

5.1. Applicability to Natural Sulfide Magmas

Our experiments were conducted with intensive parameters T, fO_2, and fS_2 that span most of the range under which sulfide magmas occur in nature. The oxygen and sulfur fugacities chosen for these experiments were selected partly for convenience, but also to reflect the conditions under which natural sulfide magmas might be expected to evolve. The initial fO_2 of a sulfide liquid will be dictated by that of its parental silicate magma at the time of sulfide liquation. Most basaltic magmas derived from the upper mantle evolve along T-fO_2 paths internally buffered by homogeneous equilibrium between dissolved Fe^{+3} and Fe^{+2} close to the QFM buffer (Carmichael and Ghiorso, 1986; Christie and Carmichael, 1986). The presence of magnetite in many sulfide ores is consistent with their evolution along a magnetite-mss cotectic, as suggested by Naldrett (1969). In rare examples such as Disko Island, Greenland (Pedersen, 1979), sulfide magmas coexist with an alloy phase, placing them near the IW oxygen buffer. In Figure 2, we show the dependence of fO_2 and fS_2 on temperature along the buffers used in this study. The conditions of our experiments are indicated by dotted vertical lines where both fO_2 and fS_2 were controlled, and by circles indicating the one buffered fugacity in the two cases in which one of them was uncontrolled. Also shown in Figure 2 is the range of fS_2 expected at the point of sulfide saturation of a basaltic magma containing 10 mol.% FeO, at either QFM or IW, calculated using relationships given by Wallace and Carmichael (1992) with a_{FeO} calculated according to Snyder and Carmichael (1992) and using thermochemical data for sulfide from Barin (1995). At QFM, the silicate melt-sulfide melt assemblage will buffer fS_2 to values near the Pt-PtS buffer (compare also with Mavrogenes and O'Neill, 1999; O'Neill and Mavrogenes, 2002). Our choice of Pt-PtS and QFM therefore provides a good approximation to conditions near the liquidus of natural sulfide magmas. At IW, the fS_2 is much lower than Pt-PtS, probably close to the conditions of experiment mss10. Silicate magmas containing much lower concentrations of FeO will reach sulfide saturation at lower values of fS_2 when they are held at a given oxygen fugacity, as shown in Figure 2.

It is worth noting here that natural sulfide ores may be somewhat richer in S than the compositions of our experiments. The discrepancy is more likely to be a result of oxygen loss from the cooling sulfide magmas rather than a tendency for natural sulfide magmas to evolve at much higher fS_2 than our experiments. The sulfur content of the sulfide liquid is dictated by the fO_2 and fS_2 at which sulfide liquid can coexist with the silicate magma from which it has exsolved. Sulfide magmas as sulfur-rich as typical solid ore assemblages could not coexist with silicate melt at the oxygen fugacities typical of silicate magmas. A perception that sulfide magmas are richer in S than our experimental compositions may also arise because ore petrologists are accustomed to recalculating their compositional data on a "100% sulfide" basis as described below, ignoring the diluting effect of magnetite despite the fact that it is an almost ubiquitous minor component of natural sulfide ore assemblages.

Table 2. Compositions of quenched sulfide liquids and coexisting mss. Only individual PGE isotope abundances used to calculate preferred partition coefficients are reported. *D* was calculated for each element as the concentration in mss divided by concentration in quenched sulfide liquid. Sd signifies one standard deviation as propogated through the calculation of *D*. Conditions are given for each experiment as temperature (°C), sulfide buffer, and oxygen buffer.

			O		Fe		Ni		S		Cu			^{102}Ru		^{103}Rh		^{108}Pd		^{193}Ir		^{195}Pt		^{197}Au	
Conds	Time (d)		Mean	sd	Mean	sd	Mean	sd	Mean	sd	Mean	sd	Totals	0.051	sd	0.025	sd	0.079	sd	0.05	sd	0.014	sd	0.01	sd
1000	2	mss6 mssxtal	0.01	0.04	54.75	0.89	4.67	0.26	36.72	0.38	3.65	0.83	99.80	25.49	2.140	31.36	1.420	4.48	0.300	27.88	2.090	4.89	0.380	1.23	0.130
Pt-PtS		mss6 melt	1.57	0.41	42.75	2.37	5.81	0.51	30.93	1.12	17.91	3.27	98.98	1.89	0.876	5.54	2.430	62.42	6.980	3.85	1.450	139.9	22.790	209.9	23.100
FMQ		D mss/melt	0.00		1.28	0.07	0.80	0.08	1.19	0.04	0.20	0.06		13.48	6.350	5.66	2.490	0.072	0.009	7.25	2.780	0.035	0.006	0.006	0.001
1000	13	mss7 mssxtal	0.00	0.00	55.55	0.22	4.49	0.05	36.86	0.22	3.00	0.12	99.89	31.67	0.587	34.7	1.160	4.05	1.770	31	1.530	3.24	0.357	0.71	0.111
Pt-PtS		mss7 melt	1.46	0.28	46.21	1.31	6.29	0.19	31.65	0.67	14.20	1.83	99.81	2.4	0.191	8.24	1.120	51.22	4.210	4.74	0.420	93.44	10.480	126.1	6.405
FMQ		D mss/melt	0.00		1.20	0.03	0.71	0.02	1.16	0.03	0.21	0.03		13.21	1.080	4.21	0.588	0.079	0.007	6.54	0.664	0.035	0.005	0.006	0.001
1050	3.5	mss8 mssxtal	0.00	0.00	56.78	0.22	3.75	0.13	36.90	0.10	2.20	0.14	99.63	27.63	3.982	33.94	2.370	9.96	1.855	30.34	3.357	7.05	2.128	2.87	2.223
Pt-PtS		mss8 melt	1.48	0.34	49.79	0.59	5.65	0.09	32.58	0.44	10.08	0.83	99.57	1.59	0.320	0		118.5	2.159	3.95	0.220	179.7	17.056	379.8	12.930
FMQ		D mss/melt	0.00		1.14	0.01	0.66	0.02	1.13	0.02	0.22	0.02		17.43	4.323	n.d.		0.084	0.016	7.68	0.951	0.039	0.012	0.008	0.006
950	4	mss9 mssxtal	0.00	0.00	54.05	0.20	4.98	0.10	36.75	0.16	4.16	0.17	99.94	56.34	5.103	46.05	2.117	3.3	0.978	48.84	3.581	2.23	0.808	1.32	0.630
Pt-PtS		mss9 melt	1.25	0.15	35.34	0.28	5.30	0.33	29.83	0.04	27.93	0.60	99.64	6.47	0.636	13.33	0.546	28.33	0.387	10.73	0.539	42.8	1.300	105.5	2.858
FMQ		D mss/melt	0.00		1.53	0.01	0.94	0.06	1.23	0.01	0.15	0.01		8.71	1.165	3.45	0.213	0.12	0.035	4.55	0.404	0.052	0.019	0.013	0.006
1000	4	mss10 mssxtals	0.00	0.01	61.35	0.18	1.62	0.02	35.71	0.17	1.71	0.22	100.40	29.32	1.476	7.72	0.494	0.370	0.072	5.700	0.278	0.170	0.016	1.840	0.129
Pt-?		mss10 melt	0.21	0.12	50.49	4.02	6.80	1.91	31.95	1.03	10.12	3.01	99.58	16.30	0.473	31.08	1.407	29.49	2.002	23.20	0.797	40.29	1.881	74.04	3.192
Fe-FeO		D mss/melt	0.01		1.22	0.10	0.24	0.07	1.12	0.04	0.17	0.05	1.01	1.80	0.105	0.25	0.019	0.012	0.003	0.25	0.015	0.004	0.002	0.025	0.002
Ni/Cu free		mss10 buffer melt	10.89	1.84	70.03	1.10	0.01	0.01	18.03	2.36	0.02	0.01	98.98												
1000	5	mss11 mss xtals	0.00	0.00	55.06	0.16	4.41	0.06	36.38	0.17	3.41	0.18	99.26	25.08	0.993	29.98	0.505	5.05	0.109	25.89	0.800	4.15	1.177	1.64	0.087
Pt-PtS		mss11 mss melt	0.39	0.18	39.37	2.73	6.92	0.71	31.64	0.83	20.27	3.88	98.58	1.86	1.169	5.93	3.048	81.90	15.520	3.58	1.825	121.30	34.499	296.40	62.160
?-FeO		D mss/melt	0.00		1.40	0.10	0.64	0.07	1.15	0.03	0.17	0.03		13.48	8.485	5.06	2.600	0.062	0.012	7.24	3.700	0.034	0.013	0.006	0.001
Ni/Cu free		mss11 buffer melt	8.73	0.86	67.58	0.09	0.01	0.01	22.08	0.77	0.01	0.01	98.42												

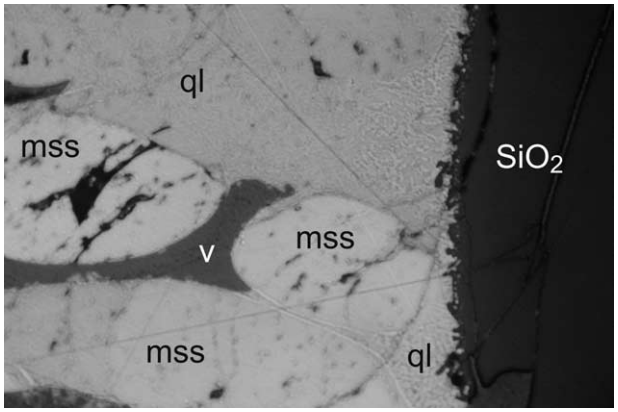

Fig. 3. Back-scattered electron micrograph of a portion of a typical run product. Phases are labeled as follows: mss = monosulfide solid solution, stable at run conditions; SiO_2 = silica glass capsule wall, coated with silica mineral; ql = trellis-textured intergrowth of sulfide minerals quenched from what was liquid at run conditions; v = vesicle created by boiling of the sulfide liquid during quench. Field of view 1 mm across.

5.2. Oxygen Contents of Sulfide Liquids

Figure 4 shows the compositions of sulfide liquids quenched in our experiments projected to the system Fe-S-O for comparison with the results of Naldrett (1969). Since sulfide liquids in five of our six experiments were cosaturated with two of the solids alloy, wüstite, magnetite or mss, these five sulfide liquids and the sulfide liquid that formed in the buffer assemblage in run mss10 are all situated exactly on cotectics, as shown.

The measured composition of sulfide liquid coexisting with FeO and alloy in experiment mss10 lies very close to the cotectic shown by Naldrett (1969), however the temperature inferred by Naldrett for such FeO-rich liquids was much higher than we have measured in our experiment. Naldrett's FeO-alloy cotectic was drawn schematically based upon known melting relations along the binary joins around the Fe-S-O ternary system and upon his measurement of the alloy-FeO-mss eutectic composition and temperature. Our determination is an actual measurement of the liquid composition at 1000°C on the FeO-alloy cotectic. We suggest that the cotectic as drawn by Naldrett (1969) is correctly placed, but that the isotherms should be moved to somewhat lower S contents. No alloy phase was observed within the Cu- and Ni- bearing sulfide melt, in the same experiment, indicating that addition of these metals would lower the temperature of formation of alloy relative to the simple Fe-S-O system.

Our Fe-S-O buffer melts contain more O than S on a molar basis, confirming the observation by Doyle and Naldrett (1987) that 'sulfide' liquids poor in Ni and Cu may commonly contain more O than S. On the other hand, even under the reducing conditions that produce Fe-S-O liquids containing as much as 27 mol.% O (i.e., more oxygen than sulfur), the coexisting Cu- and Ni-rich sulfide liquid contained as little as 0.6 mol.% O (Table 2). The oxygen content of a more oxidized Fe-Cu-Ni sulfide liquid cosaturated with magnetite and mss remains essentially constant at ~4 mol.% over the temperature range

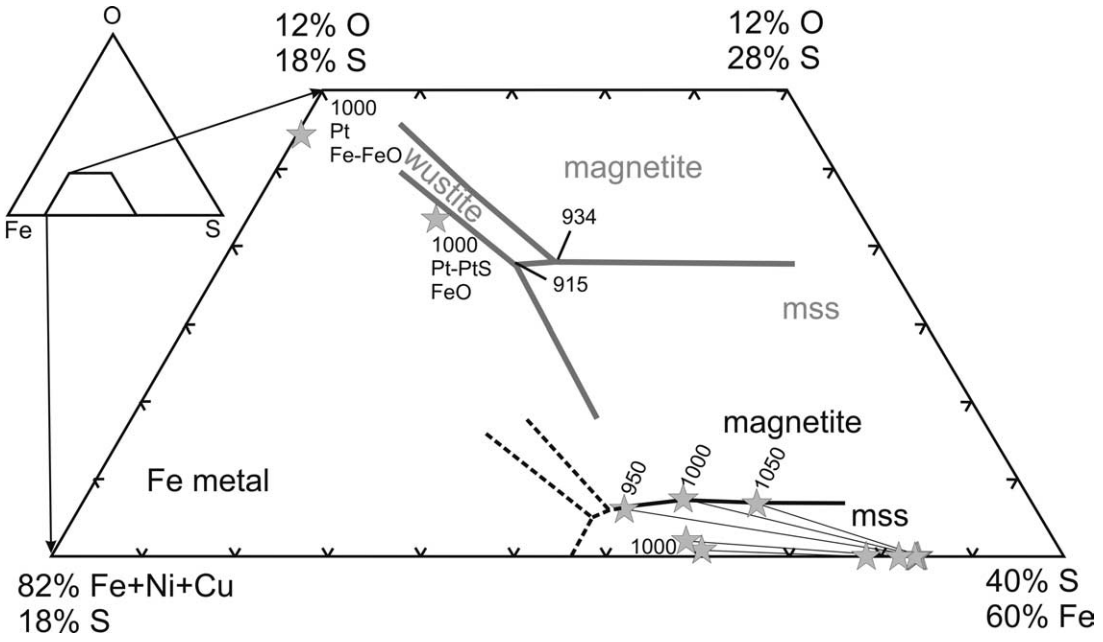

Fig. 4. Compositions of run products plotted in the (Fe+Ni+Cu)-S-O plane. Naldrett's (1969) cotectics and invariant points for the system Fe-S-O are shown in bold grey lines. Ni- and Cu-free sulfide liquids formed in the buffer assembly in the presence of wustite (labeled Fe-FeO and FeO, upper left) plot slightly outside the Naldrett's (1969) wustite field, possibly reflecting slight inaccuracy in the microprobe measurement of O concentration in the quenched sulfide liquid or minor O loss to vesicles during quench. Corresponding magnetite-undersaturated experimental liquids plot near the Fe+Ni+Cu - S join. Compositions of sulfide liquids in equilibrium with magnetite and mss are labeled with run temperatures. Tie-lines connect quenched experimental liquid compositions with those of coexisting mss.

1050 to 950°C. The magnetite-mss cotectic is thus parallel to the Fe-S join in the Cu- and Ni- rich system, as it is in the Fe-S-O system, but the addition of Cu and Ni displaces it to much lower O contents (cf. Naldrett 1969). Because this cotectic is essentially linear and parallel to the Fe-S join, coprecipitation of mss and magnetite will not tend to drive the sulfide magma to radically different fO_2 or fS_2 even under closed system conditions.

5.3. Base Metal Partitioning

The partition coefficients for Cu and Ni shown in Table 2 are similar to previously published data for the oxygen-free system Fe-Ni-Cu-S (e.g., Barnes et al., 1997). This is not surprising, in light of the exceedingly low O contents of Ni- and Cu-bearing liquids in our experiments even at fO_2 as high as QFM.

Cu is incompatible with mss under all conditions studied, which essentially span the range of T, fO_2 of natural sulfide magmas. At QFM and Pt-PtS, D_{Cu} varies from a maximum of 0.22 at 1050°C to 0.14 at 950°C. Under more reducing conditions at 1000°C, regardless of fS_2, Cu is slightly more incompatible than at QFM.

D_{Ni} varies through a considerable range but Ni remains incompatible under all conditions studied. At low fS_2 (<Pt-PtS) and low fO_2 (IW), D_{Ni} reaches a minimum value of 0.23, being nearly as incompatible as Cu. At intermediate oxygen fugacities (IW $< fO_2 <$ QFM; experiment mss11), Ni is somewhat less incompatible than Cu. At high fO_2 (QFM) and high fS_2 (Pt-PtS), D_{Ni} is much higher, and shows a moderate increase with decreasing temperature to reach a maximum of 0.90 at 950°C. It is likely that at slightly higher fS_2 or slightly lower temperature Ni would become compatible in mss, as has been shown in the oxygen-free system (e.g., Barnes et al., 1997).

5.4. Precious Metal Partitioning

The partition coefficients of the PGE and Au are shown in Table 2. Precious metal concentrations were above detection limits in all phases analyzed with the single exception of Rh in quenched sulfide liquid in experiment mss8. D_{Pt}, D_{Pd} and D_{Au} all show slight increases with decreasing temperature, but these elements remain strongly incompatible with mss under all conditions studied. D_{Ir}, D_{Ru},and D_{Rh} are all much <1 under oxidizing conditions, showing a mild decrease with decreasing temperature. A drop in fO_2 from QFM to IW $< fO_2 <$ WM at constant fS_2 (Pt-PtS) causes no significant change in D_{Ir}, D_{Ru} or D_{Rh}, whereas the combination of reductions of both fS_2 and fO_2 to below Pt-PtS and to IW causes a sharp reduction in D_{Ir}, D_{Ru}, and D_{Rh}. At low fO_2 and fS_2, Ir and Ru become incompatible in mss, raising the possibility that they may be concentrated in residual sulfide melt under unusually reducing and sulfur-poor conditions. Only Ru remains strongly compatible in mss under all conditions studied, with D_{Ru} ranging from a maximum of 14.5 to a minimum of 1.8.

5.5. Comparison to Previous Work

In Figure 5 we compare the partition coefficients for PGE and Au determined from our results with those previously published for mss/sulfide melt systems. In general the correspondence is good, and our results confirm the previously observed dependence of $D^{mss/sulfide}$on the sulfur content of the melt (Barnes et al., 2001). Our results are similar to those of Ballhaus et al. (2001) and Fleet et al. (1993, 1999a,b). The presence of oxygen as a major anion in the sulfide liquid has had little effect on $D^{mss/sulfide}$, and the sum of O + S shows a weak control on $D^{mss/sulfide}$ of the relatively incompatible elements but little effect on $D^{mss/sulfide}$ of the compatible elements Ir, Ru, and Rh. Au is the most incompatible of the precious metals, $D^{mss/sulfide}$ generally <0.01.

5.6. Fractionation of Natural Sulfide Magmas

In Figure 6 we explore some of the consequences of our observations of partitioning behavior for the evolution of sulfide magma, by comparing the results of numerical models of fractional and equilibrium crystallization of mss with a data set for massive sulfide mineralization in the Lindsley deposit of the Sudbury Igneous Complex (SIC) graciously provided by A. J. Naldrett (personal communication, 2000). Sulfide mineralization at Lindsley formed by immiscible phase separation and gravitational settling of sulfide liquid from the silicate magma of the SIC (e.g., Naldrett et al., 1999). Sulfide liquid collected at the base of the SIC to form pools which later crystallized to assemblages of pyrrhotite, chalcopyrite, pentlandite and magnetite. The geology of the Lindsley deposit and the details of analytical methods used to generate the data shown in Figure 6 are given elsewhere (Naldrett et al., 1999) and will not be repeated here. Compositional data for natural sulfides shown in Figure 6 have been normalized to 100% sulfides by assuming that all Cu is incorporated in chalcopyrite, all Ni is in pentlandite with a Fe:Ni molar ratio of 1, and all S remaining is incorporated in pyrrhotite of composition FeS. Rocks containing other minerals, such as cubanite, millerite, or bornite, may give negative amounts of pyrrhotite in the norm when this scheme is used, however the current data set does not include any such materials.

The outstanding characteristics of the data set as illustrated in Figure 6 are the presence in each plot of distinct anticorrelations between Cu and both Ni and Ir, and of strong correlation between Pt and Cu. There is a tremendous amount of scatter in the data for all elements, which must result from either late magmatic or deuteric alteration and mobilization, or alternatively from subsequent metamorphism. Either process will scatter data away from primary magmatic trends. We consider a model successful if the majority of data are found to scatter within 0.5 log units of the model trend, and unsuccessful if not. A popular interpretation of these data is to say that the Cu-poor material represents mss cumulates derived from the original sulfide liquid through a process of fractional crystallization, and the Cu-rich samples are interpreted as the residues to the removal of the cumulates. The compositional variation of sulfides at the Lindsley deposit is similar to that of well-studied Ni-Cu sulfide deposits throughout the Sudbury camp, as well as at Noril'sk (e.g., Hawley, 1965; Naldrett and Kullerud, 1967; Craig and Kullerud, 1969; Naldrett, 1969; Li et al., 1992; Naldrett et al., 1994, 1999; Zientek et al., 1994).

In Figure 6 we show the compositions of sulfide liquids that could have coexisted with a silicate melt with the probable

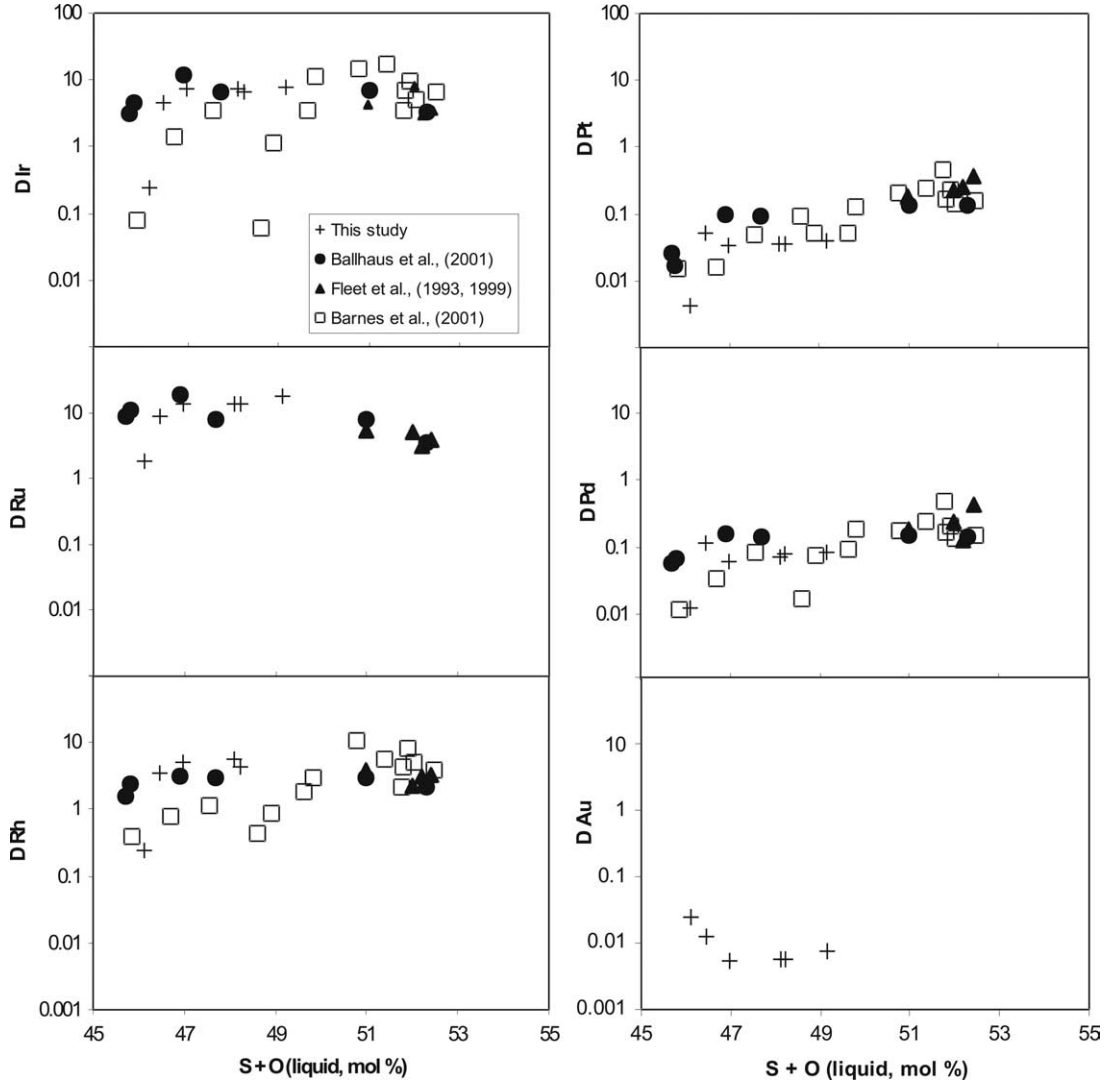

Fig. 5. Comparison of partition coefficients with published data. The partition coefficients of PGE and Au are plotted vs. the molar concentration of S + O in the sulfide liquid. Note the logarithmic scale.

average composition of the SIC before it had begun to crystallize (Mungall et al., 2004; Cu concentration estimated to be 75 ppm). The calculation was performed using the batch equilibration equation of Campbell and Naldrett (1979) and sulfide/silicate partition coefficients of 500 and 2000 for Ni and Cu, respectively, and 50,000 for Ir and Pt (cf., Peach et al., 1990; Peach and Mathez, 1993; Fleet et al., 1999a). The trend of possible initial sulfide liquids is shown with tick marks labeled at regular intervals of the mass ratio R between silicate and sulfide melts. We find that the compositions of sulfide ores are broadly accounted for at a ratio R of ~700. The model clearly does not account for the dominant trend in the data for Ni and Cu, which must therefore have resulted from another process such as crystallization of the sulfide magma during cooling.

The results of numerical models for fractional crystallization of sulfide liquid similar to composition at which the R-factor trend crosses the main cluster of data are shown in Figures 6a to 6c. The behavior of Ni is difficult to treat because of its strong dependence on temperature and oxygen fugacity. In all of our experiments, D_{Ni} was <1, but it is likely that at slightly higher fO_2 than QFM, or at slightly lower temperature than 950°C, or both, Ni will become slightly compatible. Over most of the temperature range in which fractional crystallization could occur, Ni will behave as an incompatible element. There is presently no quantitative thermodynamic model to describe the major element compositions of Fe-Ni-Cu-S-O liquids, so the evolution of a sulfide melt whose D_{Ni} depends on oxygen and sulfur content cannot be predicted with confidence. However, we can address the fractionation of sulfide magmas in a qualitative manner by assuming fractional or equilibrium crystallization with fixed partition coefficients for all elements except Ni. We use the degree of solidification as a proxy for temperature; in our scheme, D_{Ni} begins at 0.6 and increases to exceed 1 when >50% of the system has solidified.

In Figures 6a to 6c, two trend lines labeled 'cumulate' and 'liquid' indicate the instantaneous compositions of cumulate and coexisting liquid. Tick mark labels give the mass of liquid remaining at the indicated instantaneous solid and liquid com-

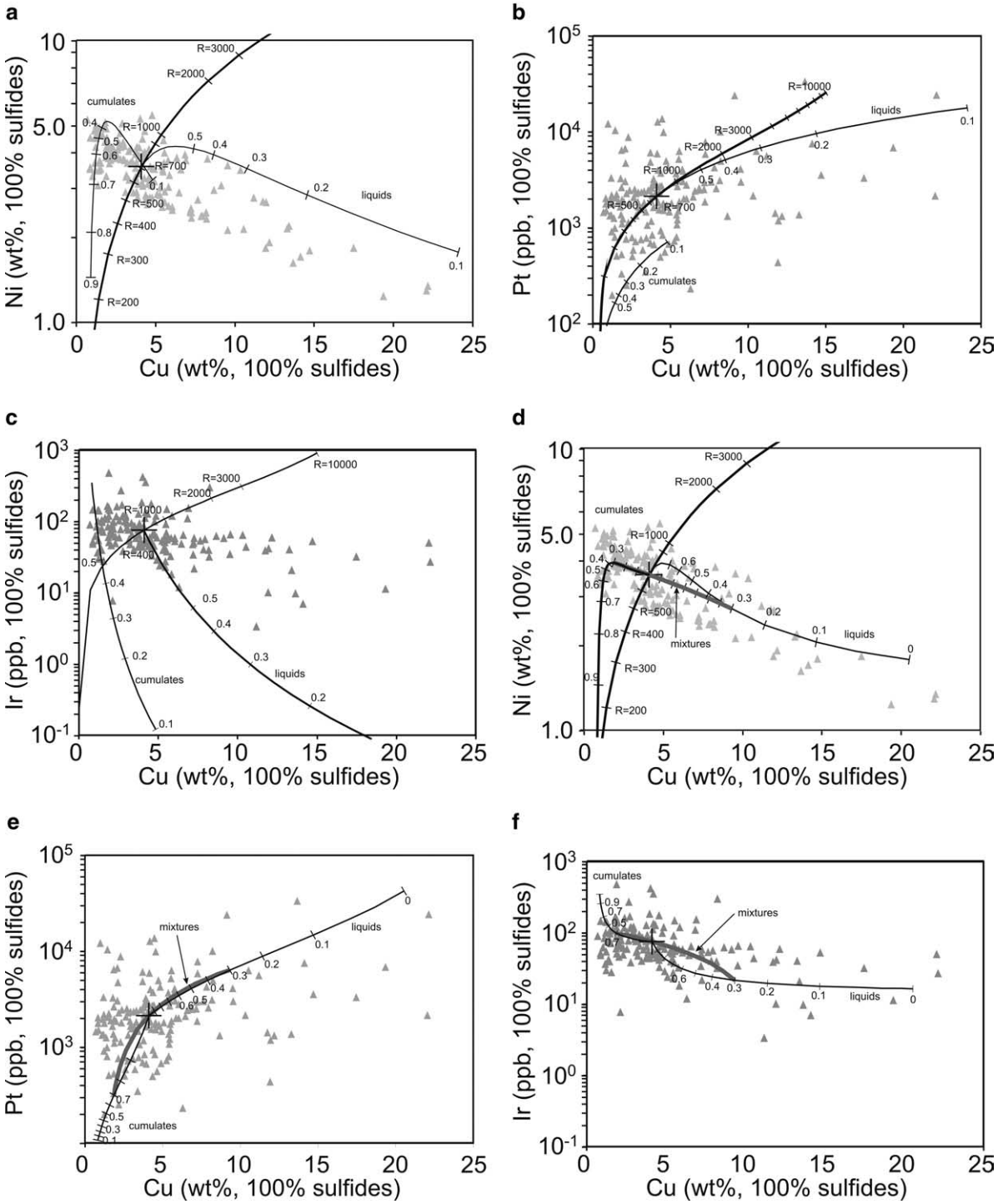

Fig. 6. model results for fractional and equilibrium crystallization of mss from a sulfide liquid similar to the Lindsley massive sulfide ore. Curves with ticks labeled $R = 200$ to $R = 3000$ show compositions of sulfide liquid that could coexist with Sudbury quartz diorite at the indicated values of silicate/sulfide mass ratio R. Liquid and cumulate trends are calculated using the Rayleigh distillation equation (ticks indicate fraction of liquid remaining) or the equilibrium crystallization equation (ticks indicate fraction of material solidified). The heavy grey trend in equilibrium models shows the compositions of mixtures of indicated proportions solids and liquids at equilibrium when 70% of the bulk system has solidified. (a) Ni vs. Cu; fractional crystallization. Ticks indicate the compositions of phases at the indicated fraction of liquid remaining. (b) Pt vs. Cu; fractional crystallization. (c) Ir vs. Cu; fractional crystallization. Ticks indicate compositions of phases at the indicated fraction of liquid remaining. (d) Ni vs. Cu; equilibrium crystallization (e) Pt vs. Cu; equilibrium crystallization. (f) Ir vs. Cu; equilibrium crystallization.

positions. It is worth pointing out that in a process of ideal fractional crystallization, the mass of the system eventually resides entirely in cumulates. The cumulate curve is therefore the locus of most of the material in the system, and one should expect to see more than half of the sulfide ore showing compositions along the portion of the cumulate curve between 1.0 and 0.4. These relationships place severe constraints upon any model for the differentiation of sulfide liquids by fractional crystallization of mss.

As is shown in Figures 6a to 6c, mss cumulates are expected to show very low concentrations of Ni, Cu and Pt, and high concentrations of Ir. Whereas 60% of the ore should contain <200 ppb Pt, there is in fact only one sample with so little of this highly incompatible element. The fractional crystallization model predicts that 60% of the ore will contain <1.5% Cu, whereas almost all samples are considerably richer in Cu. In a system evolving by fractional crystallization, a small number of samples representing the earliest-formed cumulates should contain virtually all of the Ir, and the differentiation trend in the cumulates should follow a line effectively perpendicular to the trend observed in Figure 6c. 40% of the mass of the system should consist of materials containing <10 ppb Ir, whereas in fact almost all samples contain between 30 and 200 ppb Ir.

The preferred explanation for these shortcomings in the fractional crystallization model has been that the early cumulate materials have been veined by more fractionated residual liquids, leading to the accidental sampling of material representing mechanical mixtures of cumulate and liquid (Ebel and Naldrett, 1996; Naldrett et al., 1999). If this were the case, one would expect to see large amounts of sulfide ore containing various mixutures at random between the cumulate and liquid lines. In this case, the entire area between the two lines should be scattered with data in the figures, particularly in Figure 6c. That this is not the case is a strong indication that fractional crystallization has not occurred. In other words, the early formed cumulates continued to react with the melt as they cooled, and the melt was not extracted until the cumulates had evolved to much less extreme compositions. These problems are common to all of the sulfides we have attempted to model from other deposits at Sudbury as well as the Noril'sk district. In light of the evident shortcomings of the fractional crystallization hypothesis, competing hypotheses have been advanced, including separation of sulfide liquid into two immiscible sulfide liquids (Golightly and Lesher, 1999; Ballhaus et al., 2001; Beswick, 2002), and hydrothermal rather than magmatic deposition of sulfides (Fleet, 1977).

A simple solution to the difficulties raised above is to abandon the model of fractional crystallization of mss, and propose instead that sulfide magma evolves by equilibrium crystallization to small melt fractions before any significant physical separation of crystals and liquid takes place. The ranges of possible compositions of coexisting liquid and solids during equilibrium crystallization of sulfide magma are shown in Figures 6d to 6f. The heavy gray trend lines labeled 'mixtures' show the compositions of mixtures of mss and coexisting liquid at equilibrium when 70% of the system has solidified. At such small liquid fractions, the bulk of the magma has already crystallized to a composition similar to the original bulk composition, however the solid fraction is significantly slightly richer in Ni and Ir, and slightly poorer in Cu and Pt than the bulk composition. The small amount of liquid that remains has a composition similar to the more Cu-rich sulfide samples at Lindsley. Our model of equilibrium crystallization of sulfide magma to small melt fractions duplicates the diversity of natural sulfide rocks remarkably well.

If a small mass of very late residual sulfide becomes physically separated from the cumulate mass by injection into the host rocks surrounding the sulfide body, then it will be prevented from further equilibration with the cumulates. As such a liquid passes down a temperature gradient into cooler surrounding rocks, it will crystallize. As long as it continues to migrate, it will experience fractional crystallization rather than equilibrium crystallization, permitting extreme late enrichment in the highly incompatible elements Pt, Pd and Au and depletion of the compatible elements Ir, Ru and Rh. Since this process occurs at temperatures below that at which Ni becomes a compatible element, this late process of fractional crystallization will lead to continued Ni depletion in the liquid, in contrast to the Ni enrichment expected during fractional crystallization at near-liquidus temperatures for the original sulfide magma.

It is important to note that although our models for the behavior of Ni cannot be considered to be quantitative due to uncertainties regarding the timing of changes in D_{Ni}, there is a qualitative difference between the predictions of equilibrium vs. fractional crystallization models regardless of the details of the way in which D_{Ni} is varied. The models for the other elements are much more robust because the relevant partition coefficients are very weak functions of temperature and composition. That is, even if one were to discount our arguments based on the behavior of Ni, our case still stands on the relations between Cu, Pd, and Ir. Our interpretation is limited to the temperature range at which mss is the liquidus phase in the sulfide magma; when intermediate solid solution (iss) reaches the liquidus (e.g., Craig and Kullerud, 1969) the partitioning behavior of all elements is expected to change radically. Future continuation of our experiments to lower temperatures will allow us to measure partition coefficients in iss, and to observe the nature of the transition from mss to iss crystallization.

The reason for the rather sudden transition from sulfide evolution in an essentially closed system to open system behavior and sulfide migration into the host rocks has been difficult to explain since it was first proposed that the fractionated veins were derived from the massive ores. The suggestion that it is related to a change from non-wetting to wetting behaviour of sulfide liquid against silicate phases (Ebel and Naldrett, 1996) is not supported by recent measurements of surface tension between silicate and sulfide melts (Mungall and Su, 2005). We suggest that the principal cause of the change in behavior might be the temperature of the enclosing rocks. When the silicate rocks in the outer contacts of a cooling sulfide body are above their solidus, the grains in the silicate rock will be separated by silicate melt. The very large wetting angle of sulfide liquid against oxide or silicate substrates in the presence of silicate melt prevents sulfide liquid from penetrating any partially molten silicate rock unless the sulfide is being driven through the pore space by migrating silicate melt. Once the temperature of the system has fallen below the solidus of the silicate rocks, this constraint is lifted, and sulfide liquid can migrate freely along veins or grain boundaries within the sili-

cate rocks. It may thus be the solidus temperature of the silicate host rocks to a massive sulfide orebody that dictates the degree of equilibrium crystallization attainable by the sulfide before the residual sulfide liquid can be extracted to form Cu- and PGE-rich vein deposits or haloes.

6. CONCLUSIONS

Our experimental determinations of base and precious metal partition coefficients between mss and sulfide liquid show some simple relationships that are in full agreement with preexisting results, and extend these earlier results to allow their general application to modeling of sulfide magma evolution. One important conclusion is that Ni is an incompatible element in mss under the range of fO_2 and fS_2 at which sulfide magmas are likely to exist in nature except at low temperatures near the sulfide magma solidus. Secondly, we find that Cu, Pt, Pd, and Au are incompatible in mss under all conditions. Third, we find that oxygen fugacity has little effect on the partitioning behavior of Ir, Ru and Rh, which remain strongly compatible in mss at high fS_2 over the range of fO_2 from IW to QFM. On the other hand, strong reduction of fS_2 can cause Ir and Rh to behave incompatibly in mss, allowing their concentration in residual sulfide liquids under unusually reducing and sulfur-poor conditions.

These findings can be used to show that the currently popular model of sulfide magma evolution by fractional crystallization, as generally understood, does not adequately account for the general characteristics of natural sulfide magmas. The diversity of natural sulfide compositions is much better accounted for by proposing that sulfide magmas evolve by equilibrium crystallization to temperatures near their liquidus before any significant amount of residual melt is physically separated from the solids. The last few percent of liquid, thus separated, can then migrate away from the main orebody, perhaps evolving over their last stage of evolution by fractional crystallization. The common use of a fractional crystallization model predicts variations in metal abundance that are orders of magnitude larger than observed. Our use of equilibrium crystallization models predicts model trends that are broadly in agreement with the observations. The difference between the two is more than merely semantic, because it relates to the timing of sulfide liquid migration in the cooling magmatic system. Our proposition of equilibrium crystallization to very low melt fractions requires that sulfide liquids remain trapped and immobile in their silicate hosts for much longer than is generally supposed, and has major implications for the structural and compositional aspects of ore deposits derived from fractionated sulfide magmas.

Acknowledgments—We are grateful to A. Peregoedova (McGill University and Université de Québec à Chicoutimi) for synthesis of the Po-30 standard and to J. H. G. Laflamme (CANMET) for synthesis of the Po-689 standard, preparing the polished sections and electron probe microanalyses of the standards. Claudio Cermignani provided indispensible assistance in the electron probe microanalysis of run products for major elements. James Brenan lent equipment and was always ready to discuss experimental methods. We acknowledge meticulous and constructive reviews by three anonymous reviewers and associate editor Ed Ripley.

Associate editor: E. M. Ripley

REFERENCES

Ballhaus C. and Sylvester P. (2000) Noble metal enrichment processes in the Merensky Reef, Bushveld Complex. *J. Petrol.* **41,** 545–561.

Ballhaus C., Tredoux M., and Späth A. (2001) Phase relations in the Fe-Ni-Cu-PGE-S system at magmatic temperature and application to the massive sulphide ores of the Sudbury Igneous Complex. *J. Petrol.* **42,** 1911–1926.

Barin I. (1995) *Thermochemical Data of Pure Substances*. VCH Publishers, New York.

Barnes S.-J., Makovicky E., Makovicky M., Rose-Hansen J., and Karup-Moller S. (1997) Partition coefficients for Ni, Cu, Pd, Pt, Rh and Ir between monosulfide solid solution and sulfide liquid and the formation of compositionally zoned Ni-Cu sulfide bodies by fractional crystallization of sulfide liquid. *Can. J. Earth Sci.* **34,** 366–374.

Barnes S.-J., van Achterbergh E., Makovicky E., and Li C. (2001) Proton microprobe results for the partitioning of platinum-group elements between monosulfide solid solution and sulphide liquid. *S. Afr. J. Geol.* **104,** 275–286.

Beswick A. E. (2002) An analysis of compositional variations and spatial relationships within Fe-Ni-Cu sulfide deposits on the North Range of the Sudbury Igneous Complex. *Econ. Geol.* **97,** 1487–1508.

Cabri L. J., Sylvester P. J., Tubrett M. N., Peregoedova A., and LaFlamme J. H. G. (2003) Comparison of LAM-ICP-MS and Micro-PIXE results for palladium and rhodium in selected samples of Noril'sk and Talnakh sulfides. *Can. Mineral.* **41,** 321–329.

Campbell I. H. and Naldrett A. J. (1979) The influence of silicate: sulfide ratios on the geochemistry of magmatic sulfides. *Econ. Geol.* **74,** 1503–1505.

Carmichael I. S. E. and Ghiorso M. S. (1986) Oxidation-reduction relations in basic magma: A case for homogeneous equilibrium. *Earth Plan. Sci. Lett.* **78,** 200–210.

Christie D. M., Carcmichael I. S. E., and Langmuir C. H. (1986) Oxidation states of mid-ocean ridge basalt glasses. *Earth Plan. Sci. Lett.* **79,** 397–411.

Craig J. R. and Kullerud G. (1969) Phase relations in the Cu-Fe-Ni-S system and their application to magmatic ore deposits. *Econ. Geol. Monogr.* **4,** 344–358.

Distler V.V., Malevskiy A. Yu., and Laputina I. P. (1977) Distribution of platinoids between pyrrhotite and pentlandite in crystallization of a sulfide melt. *Geochem. Int.* **14,** 30–40.

Doyle C. D. and Naldrett A. J. (1987) The oxygen content of "sulfide" magma and its effect on the partitioning of nickel between coexisting olivine and molten ores. *Econ. Geol.* **82,** 208–211.

Ebel D. S. and Naldrett A. J. (1996) Fractional crystallization of sulfide ore liquids at high temperature. *Econ. Geol.* **91,** 607–621.

Fleet M. E. (1977) Origin of disseminated copper-nickel sulfide ore at Frood, Sudbury, Ontario. *Econ. Geol.* **72,** 1449–1456.

Fleet M. E. and Stone W. E. (1991) Partitioning of platinum-group elements in the Fe-Ni-S system and their fractionation in nature. *Geochim. Cosmochim. Acta* **55,** 245–253.

Fleet M. E. and Pan Y. (1994) Fractional crystallization of anhydrous sulfide liquid in the system Fe-Ni-Cu-S, with application to magmatic sulfide deposits. *Geochim. Cosmochim. Acta* **58,** 3369–3377.

Fleet M. E., Chryssoulis S. L., Stone W. E., and Weisener C. G. (1993) Partitioning of platinum-group elements and Au in the Fe-Ni-Cu-S system: Experiments on the fractional crystallization of sulfide melt. *Contrib. Mineral. Petrol.* **115,** 36–44.

Fleet M. E., Crocket J. H., Liu M., and Stone W. E. (1999a) Laboratory partitioning of platinum-group elements (PGE) and gold with application to magmatic sulfide-PGE deposits. *Lithos* **47,** 127–142.

Fleet M. E., Liu M., and Crocket J. H. (1999b) Partitioning of trace amounts of highly siderophile elements in the Fe-Ni-S system and their fractionation in nature. *Geochim. Cosmochim. Acta* **63,** 2611–2622.

Golightly J. P. and Lesher C. M. (1999) MSS fractionation, volatile-enhanced partitioning and sulphide liquid immiscibility in magmatic Fe-Ni-Cu-(PGE) sulphide deposits. *Geol. Assoc. Can.-Mineral. Assoc. Can. Progr. Abstr.* **24,** 4619.

Hawley J. E. (1965) Upside-down zoning at Frood, Sudbury, Ontario. *Econ. Geol.* **60,** 529–575.

Kress V. (1997) Thermochemistry of sulfide liquids. I. The system O-S-Fe at 1 bar *Contrib. Mineral. Petrol.* **127,** 176–186.

Li C., Naldrett A. J., Coats C. J. A., and Johannessen P. (1992) Platinum, palladium, gold and copper-rich stringers at Strathcona Mine, Sudbury: Their enrichment by fractionation of a sulfide liquid. *Econ. Geol.* **87,** 1584–1596.

Li C., Barnes S.-J., Makovicky E., Rose-Hansen J., and Makovicky M. (1996) Partitioning of nickel, copper, iridium, rhenium, platinum and palladium between monosulfide solid solution and sulfide liquid: Effects of composition and temperature. *Geochim. Cosmochim. Acta* **60,** 1231–1238.

Longerich H. P., Jackson S. E., and Günther D. (1996) Laser ablation-inductively coupled plasma mass spectrometric transient signal data acquisition and analyte concentration calculation. *J. Anal. Atom. Spectrom.* **11,** 899–904.

MacLean W. H. (1969) Liquidus phase relations in FeS-FeO-Fe_3O_4-SiO_2 system and their application to geology. *Econ. Geol.* **64,** 865–884.

Makovicky E (2002) Ternary and quaternary phase systems with PGE. In *The Geology, Geochemistry, Mineralogy and Mineral Beneficiation of Platinum-Group Elements* (ed. L. J. Cabri).

Mavrogenes J. A. and O'Neill H. S. (1999) The relative effects of pressure, temperature and oxygen fugacity on the solubility of sulfide in mafic magmas. *Geochim. Cosmochim. Acta* **63,** 1173–1180.

Mungall J. E., Ames D. A., and Hanley J. J. (2004) Geochemical evidence from the Sudbury structure for crustal redistribution by large bolide impacts. *Nature* **429,** 546–548.

Mungall J. E. and Su S. (2005) Interfacial tension between magmatic sulfide and silicate liquids: Constraints on kinetics of sulfide liquation and sulfide migration through silicate rocks. *Earth Planet. Sci. Lett.* **234,** 135–149.

Naldrett A. J. (1969) A portion of the system Fe-S-O between 900 and 1080°C and its application to sulfide ore magmas. *J. Petrol.* **10,** 171–202.

Naldrett A. J. and Kullerud G. (1967) A study of the Strathcona Mine and its bearing on the origin of the nickel-copper ores of the Sudbury District, Ontario. *J. Petrol.* **8,** 453–531.

Naldrett A. J., Asif M., Gorbachev N. S., Kunilov V. Ye., Stekhin A. I., Fedorenko V. A., and Lightfoot P. C. (1994) The composition of the Ni-Cu ores of the Oktyabr'sky Deposit, Noril'sk Region. *Ont. Geol. Surv. Spec. Vol.* **5,** 357–371.

Naldrett A. J., Asif M., Schandl E., Searcy T., Morrison G. G., Binney W. P., and Moore C. (1999) Platinum-group elements in the Sudbury ores: Significance with respect to the origin of different ore zones and to the exploration for footwall ore bodies. *Econ. Geol.* **94,** 185–210.

O'Neill H. S. and Mavrogenes J. A. (2002) The sulfide capacity and the sulfur content at sulfide saturation of silicate melts at 1400°C and 1 bar. *J. Petrol.* **43,** 1049–1087.

Peach C. L., Mathez E. A., and Keays R. R. (1990) Sulfide-silicate melt distribution coefficients for noble metals and other chalcophile elements as deduced from MORB: Implications for partial melting. *Geochim. Cosmochim. Acta* **54,** 3379–3389.

Pedersen A. K. (1979) Basaltic glass with high-temperature equilibrated immiscible sulphide bodies with native iron from Disko, Central West Greenland. *Contrib. Mineral. Petrol.* **69,** 397–407.

Snyder D. A. and Carmichael I. S. E. (1992) Olivine-liquid equilibria and the chemical activities of FeO, NiO, Fe2O3 and MgO in natural basic melt. *Geochim. Cosmochim. Acta* **56,** 303–318.

Sylvester P. J. (2001) A practical guide to platinum-group element analysis of sulfides by laser ablation ICPMS. In *Laser-Ablation-ICPMS in the Earth Sciences, Principles and Applications* (ed. P. Sylvester), Min. Assoc. Canada, Short Course **29,** Chap. 13, 203–211.

Wallace P. and Carmichael I. S. E. (1992) Sulfur in basaltic magmas. *Geochim. Cosmochim. Acta* **56,** 1863–1874.

Wilson S. A. Ridley W. I., and Koenig A. E (2002) Development of sulfide calibration standards for the laser ablation inductively-coupled plasma mass spectrometry technique. *J. Anal. Atom. Spectrom.* **17,** *4,* 406 – 409.

Zientek M. L., Likhachev A. P., Kunilov V. E., Barnes S.-J., Meier A. L., Carlson R. R., Briggs P. H., Fries T. L. and Adrian B. M (1994) Cumulus processes and the composition of magmatic ore deposits: Examples from the Talnakh District, Russia. *Ont. Geol. Surv. Spec. Vol.* **5,** 373–392.